Journal of Applied Physics

Study of the SET switching event of VCM-based memories on a picosecond timescale

Cite as: J. Appl. Phys. **127**, 204501 (2020); https://doi.org/10.1063/5.0003840
Submitted: 05 February 2020 . Accepted: 07 May 2020 . Published Online: 22 May 2020

M. von Witzleben, T. Hennen, A. Kindsmüller, S. Menzel, R. Waser, and U. Böttger

Journal of Applied Physics ARTICLE scitation.org/journal/jap

Study of the SET switching event of VCM-based memories on a picosecond timescale

Cite as: J. Appl. Phys. **127**, 204501 (2020); doi: 10.1063/5.0003840
Submitted: 5 February 2020 · Accepted: 7 May 2020 ·
Published Online: 22 May 2020

M. von Witzleben,[1,a)] T. Hennen,[1] A. Kindsmüller,[1] S. Menzel,[2] R. Waser,[1,2,3] and U. Böttger[1]

AFFILIATIONS

[1]Institut für Werkstoffe der Elektrotechnik 2, RWTH Aachen University, Sommerfeldstraße 24, D-52074 Aachen, Germany
[2]Peter Grünberg Institut 7, Forschungszentrum Jülich and JARA-FIT, Wilhelm Johnen Straße, D-52428 Jülich, Germany
[3]Peter Grünberg Institut 10, Forschungszentrum Jülich and JARA-FIT, Wilhelm Johnen Straße, D-52428 Jülich, Germany

[a)]**Author to whom correspondence should be addressed:** witzleben@iwe.rwth-aachen.de

ABSTRACT

In this paper, we present an approach of measuring the SET kinetics of redox-based resistive memories at timescales below 100 ps. Automatic measurements with an RF pulse generator and a source measure unit allow the consecutive application of short electrical pulses and the precise detection of the device resistance. In addition, a statistical evaluation of the SET kinetics has been performed. By increasing the pulse duration in small steps, varying the pulse amplitude and collecting a comprehensive dataset, the transient resistance of a device can be determined at a picosecond timescale. With this setup, we measured the SET kinetics of two different valence change memory-based resistive switching oxides, namely, TaO_x and ZrO_x, between 50 ps and 250 ps. Two characteristic times were measured: the SET time, being the delay after which the transition to the low resistance state sets in, and the transition time, which is the timespan during which the resistance shifts from the high to the low resistive state. We measured SET times down to 50 ps and transition times below 15 ps for both materials. The intrinsic maximum switching speed is not reached yet, which is limited by the ion migration in the oxides, possibly corresponding to the phonon THz frequency. Although charging times and heating times potentially slow down the measured SET times, they still allow 50 ps writing times at voltages of less than 5.0 V.

I. INTRODUCTION

Redox-based resistive memories (ReRAMs) have, among other emerging memory technologies, a high potential to successfully address the technological barriers that conventional computing architectures face.[1,2] It features not only high endurance,[3] long retention,[4] high scalability,[5] and fast writing times,[6–11] but also the potential to be used for neuromorphic applications or in-memory computing.[12] The information of a ReRAM device is stored in its resistive value, which can be programed by electrical stimuli. It is switched between either two binary states, namely, the high resistive state (HRS) and the low resistive state (LRS), or between multiple resistive states.[13] This work focuses on valence change memories (VCMs), which are realized by placing a thin transition metal oxide, e.g., TaO_x or ZrO_x, layer between two metallic electrodes. The change of resistance results from a rearrangement of ionic defects, typically oxygen vacancies, within a confined conductive filament, which has been resolved in several spectroscopic studies.[14–17] For HfO_x devices, it has been shown that this filament has a diameter between 1 nm and 3 nm.[18] Usually, one of the two electrodes consists of an inert metal and is referenced to as active electrode (AE), as the switching is assumed to take place at its interface. The other one has a high oxygen affinity and forms an ohmic contact. In the LRS, the filamentary region near the AE is rich in oxygen vacancies, which leads to a good electrical conductivity.

During the application of a voltage, the current density J reaches its maximum in the filament, due to its small cross section. Also, most of the voltage drops over the oxide layer, which leads to a large electrical field E within the filament. Both J and E heat up the filament by Joule heating. The corresponding dissipated power density is $Q = J \cdot E$. The increased temperatures, in turn, increase the mobility of oxygen vacancy significantly and, thereby, facilitate their drift movements in the filament.[19] During the RESET (transition from LRS to HRS), oxygen vacancies are repelled from the AE and thereby decrease the electrical conductivity. As the oxygen vacancy concentration decreases near the AE, a diffusion current of oxygen vacancies sets in, opposite to the drift current. Subsequently, both currents reach an equilibrium and the oxygen

vacancy distribution remains constant within the filament.[20] During the SET from the HRS to the LRS, the Joule heating occurs in the filamentary region near the AE, which triggers a thermal runaway.[19] This increase in temperature has been confirmed in several experimental studies.[21–23] Consequently, they migrate rapidly toward the AE and enhance the electrical conductivity significantly in this region. Several simulation studies succeeded to model the characteristic *I–V* curves of VCM devices on the basis of oxygen migration.[24–26]

Many studies have analyzed the switching speed down to few nanoseconds.[19–20,27–30] Pioneering work in the sub-nanosecond regime has been performed by Torrezan *et al.*[6] They built a broadband setup consisting of a real-time oscilloscope and a 100 ps pulse generator. With this setup, they were able to SET the device within 105 ps and to RESET it within 120 ps. This setup was used in other studies to show similar fast switching times in Pt-doped SiO_2[7] and 85 ps fast switching times in AlN devices.[8] To our knowledge, this is the fastest switching time reported for a VCM-based device. A challenge for ReRAM devices to overcome is the voltage time dilemma:[1] At high voltages, fast switching times are desired. At low voltages, however, long data retention is desired to prevent the device from switching during the read-out. In our recent publication, it has been demonstrated that a Pt/TaO_x/Ta device is able to address the voltage time dilemma by studying its SET kinetics from 250 ps to 10^4 s.[11] The origin of this non-linear dependence of the SET time on the applied voltage is attributed to the Joule heating in the filamentary region near the AE,[19,29,31,32] which can occur within less than 120 ps.[10] Furthermore, it could be proven that the switching speed is not limited by intrinsic processes but by the charging of the device capacitance.[11] The latter was already predicted by the circuit-based model of Lu *et al.*[33]

Here, we focus on the voltage dependent SET kinetics of Pt/TaO_x/Ta and Pt/ZrO_x/Ta devices in the regime from 50 ps to 250 ps. So far, no study compared two different VCM devices on a sub-nanosecond timescale. As Zr is chemically similar to Hf, also similar switching kinetics are expected for HfO_x based devices.[34] However, only the RESET kinetics of HfO_x based devices were studied on a sub-nanosecond regime.[9] No publication exists on the switching kinetics of ZrO_x based devices in the sub-nanosecond regime. For TaO_x devices, an endurance of up to 10^{12} cycles[3] has been shown and for HfO_x devices of up to 10^9 cycles.[35] The endurance of ZrO_x devices has not yet been studied this thoroughly and only 10^4 cycles have been reported so far.[16]

To determine the SET time, two evaluation methods exit: (i) In the first approach, the transmitted signal is evaluated and the time at which the current increases starts is taken as the SET time. This approach is used for SET kinetic measurements at time timescales above 100 ns.[29,31,36] At faster timescales, however, this approach leads to unprecise results, as the SET time becomes shorter than the charging time of the capacitances.[11] (ii) In the second approach, only the width of the transmitted signal is evaluated. This method is used in the sub-nanosecond regime.[6–8,11] The exact SET time, however, can be faster than the pulse width. Compared to method (i), the determination of the SET time with method (ii) is less complex.

To circumvent the disadvantages of both methods, we measured a more comprehensive data set. Similarly to method (ii), the pulse width and the device resistance before and after the application of the pulse were determined. Opposite to previous studies using method (ii),[6–8,11] this cycle was conducted about 1000 times (970 times for the TaO_x and 1010 times for the ZrO_x device, cycle numbers are explained in Sec. III). Additionally, the pulse width and amplitude were varied. With this comprehensive data set, the transient change in resistance is resolved similarly to Ref. 19, but on a picosecond timescale. This allows the precise determination of the SET time in the regime between 50 ps and 250 ps. The transition time can even be detected on a faster timescale.

II. EXPERIMENTAL

The devices used in this paper were embedded in a coplanar waveguide structure consisting of 30 nm thick Pt lines. This structure provides proper impedance matching at the connection between the probes and the device, as the substrate served a high resistive Si-Wafer ($\rho > 10\,k\Omega\,cm$) with a 430 nm thick SiO_2 layer. The deposition process of the films is identical to the ones presented in Ref. 37 (ZrO_x) and Ref. 38 (TaO_x). All materials were deposited by means of radiofrequency magnetron sputtering. The bottom electrode consists of a 5 nm thick Ti adhesion layer and a 30 nm thick Pt layer, which serves as waveguide and active bottom electrode. The active switching material either 5 nm TaO_x or 5 nm ZrO_x were deposited. The top electrode consists of 20 nm Ta, forming the ohmic electrode of the ReRAM device, and 30 nm of Pt, constituting the continuation of the coplanar waveguide. Both, the bottom and top electrodes, were structured with optical lithography and a lift-off process. The outer conductors of the CPW structure consist of the materials of the top electrode. The width of the inner conductor is 100 μm and has a spacing of 60 μm to the outer conductors. Toward the ReRAM device, its width is gradually reduced to 2 μm and the spacing to 1.5 μm. The intersection of both electrodes is $2 \times 2\,\mu m^2$.

Frequency domain measurements of the coplanar waveguide structure up to 40 GHz are shown in the supplementary material (Fig. S1). The forward transmission is always higher than −3 dB, meaning that more than 70% of the signal is transmitted through the coplanar waveguide. The transmission, however, is slightly lower than the transmission of the coplanar waveguides presented in Ref. 6, which is attributed to the thinner Pt layer in our study (200 nm in Ref. 6). The capacitances of both devices were measured with a HP4284A LCR-Meter at a frequency of 1 MHz and a stimulus of 50 mV. The capacitance amounts to 0.38 pF for the TaO_x and to 0.29 pF for the ZrO_x device. Calculating the capacitances (assuming a parallel plate capacitor) with the dielectric constants of 26[39] (TaO_x) and 28.5[40] (ZrO_x) results in 0.18 pF (TaO_x) and 0.20 pF (ZrO_x). The deviation of the measured capacitance from the theoretical one is assumed to originate from the additional capacitances from the substrate and from parasitic angular capacitances. With the measured line resistance of 150 Ω, these small capacitances result in short charging times around 50 ps. All voltages indicated in this paper are applied to the Ta top electrode.

The devices were formed by applying a 0.5 V/s ramp with an amplitude of 4 V using a Keithley 2634B SMU and a current compliance of 100 μA. Exemplary *I–V* sweeps of both devices were measured at a sweep rate of 0.5 V/s and are shown in Fig. 1.

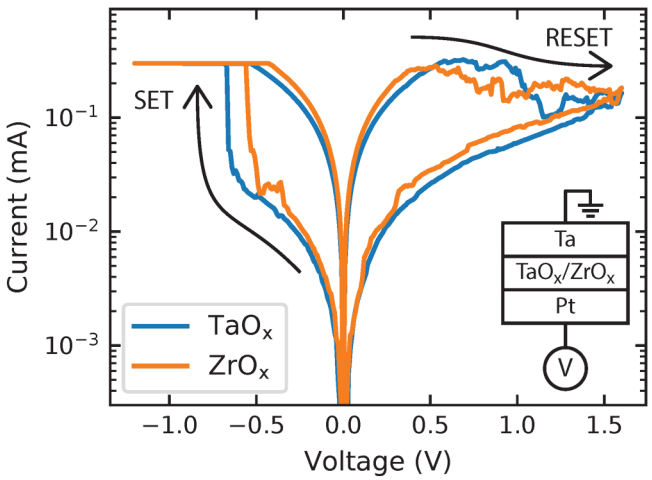

FIG. 1. Exemplary *I-V* sweeps (sweep rate: 0.5 V/s) of the TaO_x (blue) and the ZrO_x (orange) device.

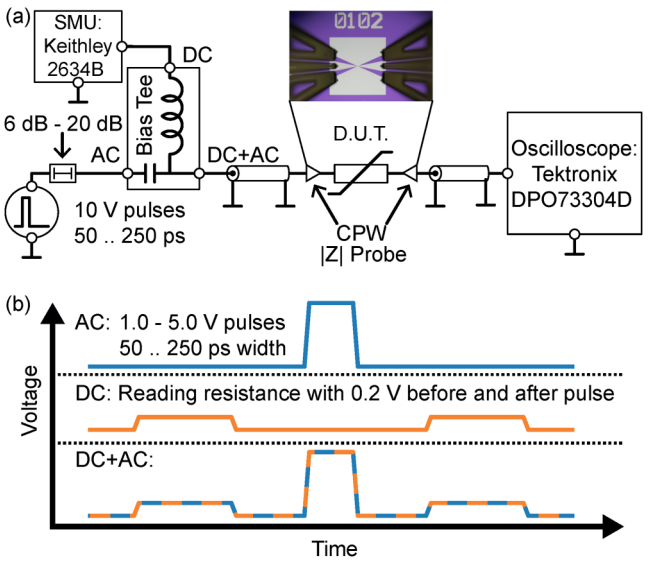

FIG. 2. (a) Schematic of the setup. The capacitor and the coil simplify the AC and DC entry of the bias tee. A microscopic picture of the probe and the sample is shown in the inset. (b) Illustration of measurement cycle. A voltage pulse (upper blue line) with an amplitude between −1.00 V and −5.01 V and a duration of 50 ps to 250 ps is applied to the device. Before and after the application of the pulse, the SMU measures the resistance at the DC entry with a voltage of −0.2 V (intermediate orange line). Both signals are combined at the DC + AC output of the bias tee (lower orange blue dashed line).

Capacitive charging and the heating of the devices occur on a much faster timescale than the sweep rate and can, therefore, be neglected during these measurements. The capacitive charging time is around 50 ps (as shown above) and the heating time of ReRAM devices is below 120 ps.[10] The mean SET voltage of 410 cycles amounted to 0.75 V for the TaO_x and to 0.64 V for the ZrO_x device. The lower SET voltage of the ZrO_x device is attributed to its lower migration barrier for oxygen vacancies. For yttria-stabilized ZrO_x with low yttrium concentrations, the migration barrier is always below 0.6 eV.[41] In TaO_x, in contrast, the migration barrier is reported to be above 1 eV.[42,43] In addition, different thermal conductivities in ZrO_x and TaO_x could influence the temperature in the device and, thereby, have an effect on the SET voltage.

An endurance of up to 10^6 cycles for the TaO_x device, has already been shown.[44] For the ZrO_x device, only an endurance of up to 10^4 cycles was reported so far.[16] Therefore, an additional endurance measurement on a $5 \times 5\,\mu m^2$ crossbar device has been conducted. The fabrication process was identical to one of the ZrO_x devices used in this study, except for the mask. As shown in the supplementary material (Fig. S2), an endurance of up to 10^6 cycles has been achieved.

The experimental setup is sketched in Fig. 2(a). A custom pulse generator from the Sympuls GmbH generates pulses with an amplitude of 5 V (at 50 Ω impedance) with a tunable pulse width between 50 ps and 250 ps. Two exemplary pulses are shown in the supplementary material (Fig. S3). Those pulses are transmitted through a broadband bias tee (API 8810KFM3-40) from the AC to the AC + DC connections. The sample is connected with a Z-probe from Cascade Microtech. The transmitted signal is measured with a real time oscilloscope Tektronix DPO73304D (Bandwidth: 33 GHz, Sample rate: 100 GS/s). At the DC entrance of the bias tee, a Keithley 2634B SMU is connected. The bias tee allows us to combine both the signal at the AC and at the DC entrance as shown in Fig. 2(b) with a neglectable cross-talk between the AC and the DC channel. All components including the bias tee are designed for frequencies up to 40 GHz. To verify that the pulse width is preserved over the transmission line, pulses with a full width have maximum (FWHM) of 50 ps and 250 ps were applied to the ZrO_x device in the LRS (550 Ω). The transmitted voltage (Fig. S4 in the supplementary material) is attenuated due to the relatively high resistance (>50 Ω impedance) of the device, but its FWHM is preserved. So, it is possible to measure the device resistance precisely with an SMU and to apply short pulses with this setup. The current of the SMU also flows into the scope and, therefore, the 50 Ω impedance needs to be subtracted from the measured resistance values.

As the 50 Ω transmission line is not properly terminated at the device, most of the signal is reflected and, therefore, the effectively applied voltage doubles at the device. This is a result of the superposition of the incoming and the reflected signal. The effective pulse voltage V_P (two times the pulse voltage of the generator) is used throughout this paper.

The static resistance of the device is read with a voltage of −0.2 V before and after the application of the short SET pulse. The resistance before the application is referenced to as R_{LRS} and the one after the application as R_{HRS}. Each cycle ends with a voltage sweep with a SET voltage of −1.2 V and a RESET voltage of 1.6 V (Sweep rate: 0.5 V/s), which brings the device in its initial HRS state. This is done to reinitialize the device in a similar state for each cycle and to test whether the cell is still switching. During the SET sweeps, a current compliance of 300 μA is used. The pulse

width is varied from 50 ps to 250 ps in steps of 5 ps and each cycle is repeated 10 times. This measurement is repeated with different broadband attenuators between the pulse generator and the bias tee. Thereby, the effective pulse voltage V_P can be adjusted between −10.00 V without attenuation and −1.00 V with an attenuation of 20 dB. The used attenuation values are 6 dB (−5.01 V), 10 dB (−3.16 V), 13 dB (−2.24 V), 16 dB (−1.58 V), and 20 dB (−1.00 V).

The distribution of the R_{HRS} is shown in Fig. S5 in the supplementary material. The R_{HRS} distribution of the ZrO_x device scatters between 5 kΩ and 100 kΩ, whereas one of the TaO_x devices scatters between 10 kΩ and 50 kΩ. In a recent study, we have shown that R_{HRS} strongly influences the SET time for HfO_x devices.[45] To reduce this influence, cycles were discarded in the evaluation if their R_{HRS} value was not within the resistance window between 10 kΩ and 30 kΩ. To maintain the amount of statistics, the discarded cycles were repeated. The mean R_{HRS} values within this resistance window amount to 23.83 ± 3.73 kΩ for the TaO_x device and to 22.18 ± 4.77 kΩ for the ZrO_x device.

III. RESULTS AND DISCUSSION

The measurements of the TaO_x device at $V_p = -2.24$ V are shown as a box plot in Fig. 3(a). The FWHM indicated on the abscissa was calculated by interpolating the measured transmitted signals. The ratio R_{LRS}/R_{HRS} is distributed narrowly around unity at shorter pulse durations, showing that the applied pulse has no effect on the device's resistance. However, at 90 ps, the box plot broadens, and at 100 ps, the median values begin to drop. The broadening of the box plot indicates that the occurrence of a switching event to the LRS occurs randomly at this pulse duration. At pulse durations above 120 ps, the device always switches to the LRS. The measurements of the ZrO_x device, also at $V_p = -2.24$ V, are shown in Fig. 3(b). At 50 ps, the median of the ratio R_{LRS}/R_{HRS} is at unity indicating that at most of the 50 ps pulses the device did not switch to the LRS. At 60 ps, the median of the ratio R_{LRS}/R_{HRS} is below 0.1, and the device switched to the LRS at every cycle. As the devices never switched completely to the LRS at 50 ps, but always at 60 ps, the transition from the HRS to LRS needs to occur within the additional 10 ps. The box plot representation of all measurements can be found in the supplementary material (Figs. S6 and S7) along with the distributions of the R_{LRS} values (Figs. S8 and S9).

The median values of the ratio R_{LRS}/R_{HRS} at all measured voltages are shown in Fig. 3(c). To reduce the stress on the devices, measurements with higher pulse amplitude were aborted as soon as a pulse duration was reached at which the devices switched to the LRS at each cycle. This resulted in 970 cycles for the TaO_x and 1010 cycles for the ZrO_x device. Both devices remained operational during all conducted measurements. The TaO_x and the ZrO_x devices switched to the LRS already at a FWHM of 50 ps at $V_p = -5.01$ V and $V_p = -3.16$ V, respectively. Exemplary transmitted pulses of this measurement are shown in Figs. 4(a) and 4(b). The FWHM is even below 50 ps, which is due to capacitive effects and does not imply that the electrical stimulus seen by the device was shorter than 50 ps. At lower voltages, both devices switched within 55 ps to 145 ps. At $V_p = -1.58$ V ($V_p = -1.00$ V), the TaO_x (ZrO_x) device did not switch at any pulse width.

At lower voltages and longer pulse widths, the SET event is visible in the transmitted signal as demonstrated in Fig. 4(c) for the ZrO_x device. Therefore, deriving the SET time from this transmitted signal using method (i) (introduced in Sec. I) is possible. The applied pulse had an amplitude of $V_p = -1.58$ V and a FWHM of

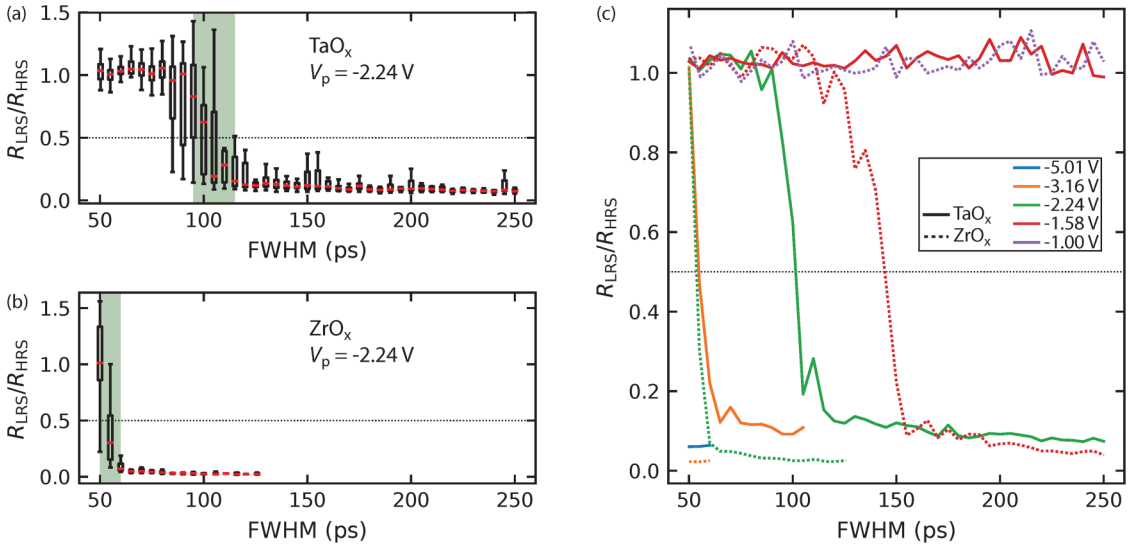

FIG. 3. Boxplots of the ratio R_{LRS}/R_{HRS} at different pulse widths for TaO_x (a) and the ZrO_x device (b). The pulse amplitude was $V_p = -2.24$ V. The green shaded area indicates the determined transition time. (c) The median values of R_{LRS}/R_{HRS} at different pulse amplitudes in dependence of the pulse width. The green curves at $V_p = -2.24$ V correspond to the median values in (a) and (b).

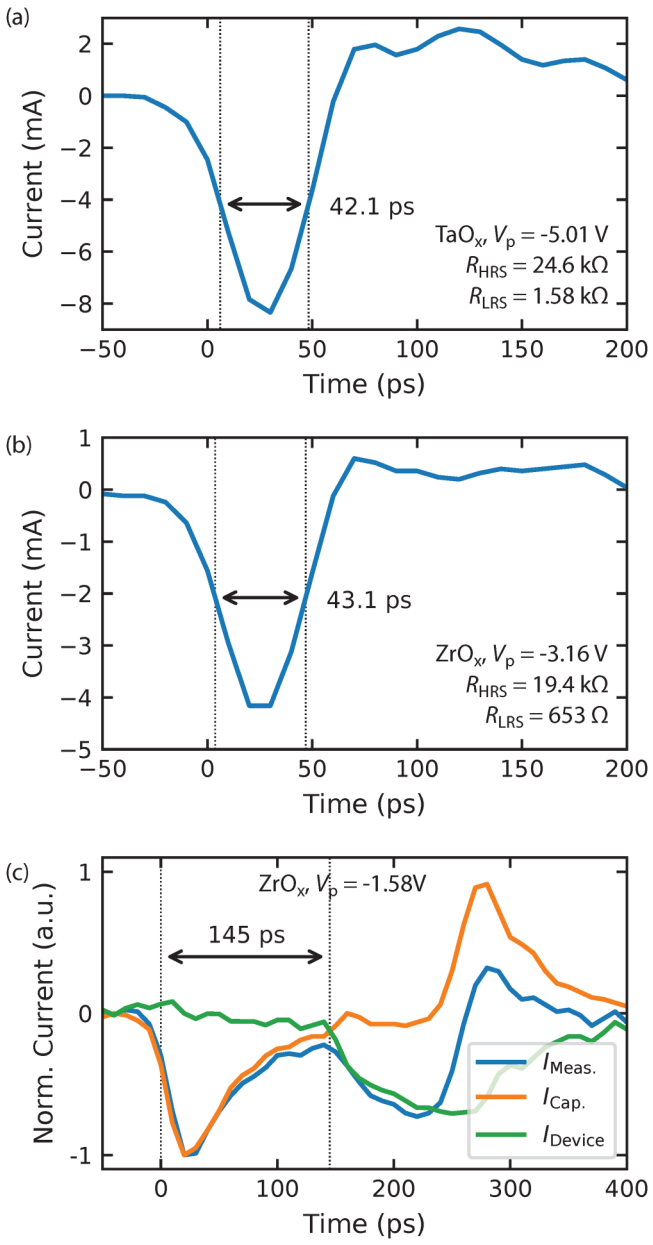

FIG. 4. Transmitted current of the (a) TaO_x and the (b) ZrO_x device of a 50 ps pulse. During this excitation, both devices switched from the HRS to the LRS. (c) Normalized transmitted current (blue) of a ZrO_x device at a pulse width of 250 ps and a pulse amplitude of $V_p = -1.58$ V. Corresponding capacitive current (orange) and difference between both (green). The difference corresponds to the normalized current through the device. Its increase after 145 ps corresponds to the SET event.

250 ps. The measured normalized current $I_{Meas.}$ is shown as a blue curve. This curve, however, is a superposition of the capacitive current and the current through device. To separate both, the capacitive current needs to be determined and subtracted. As during a pulse with an amplitude of $V_p = -1.00$ V no switching occurs, this current corresponds to the capacitive current. Therefore, the normalized capacitive current I_{Cap} (orange) is subtracted from I_{Meas}, which results in the effective normalized current through the device I_{Device} (green). At the beginning, the device is highly resistive and no current flows through the device. It increases abruptly after about 145 ps, corresponding to the SET time.

A similar SET time is derived with method (ii) for the ZrO_x device at $V_p = -1.58$ V [see red-dashed curve in Fig. 3(c)]. Here, the resistance of the ZrO_x device drops also after about 145 ps, showing that both evaluation methods yield similar results for the SET time. As method (i) not only becomes unreliable at timescales in the range of the capacitive charging time, but is also more complex, in the following only method (ii) is used to determine the SET time. The use of the comprehensive data set allows us to determine the SET time and the transition time at a temporal resolution below 15 ps with this method.

The SET time is defined as the pulse width at which the median of the ratio R_{LRS}/R_{HRS} drops below 0.5. The resulting SET times are shown in Fig. 5(a). The transition time from the HRS to the LRS is also determined from the median values of the ratio R_{LRS}/R_{HRS} and shown in Fig. 5(b). It is defined here as the timespan between the last value of R_{LRS}/R_{HRS} above 0.8 and the first below 0.2. Two exemplary transitions are marked as the green shaded area in Figs. 3(a) and 3(b). The ZrO_x device has faster SET and transition times than the TaO_x device at all effective pulse voltages.

Two explanations exist for the faster SET and transition times of the ZrO_x device. The first (a) is its lower SET voltage, which is attributed to the lower migration barrier for oxygen vacancies as explained above. The second (b) is the difference between the mean R_{HRS} value of the ZrO_x device (22.18 ± 4.77 kΩ) and the mean R_{HRS} value of the TaO_x devices (23.83 ± 3.73 kΩ). As a lower R_{HRS} yields a faster SET time,[45] this could explain the faster SET times of the ZrO_x device. To investigate possibility (b), we performed the identical analysis as above on cycles of the ZrO_x device, in which the R_{HRS} values are between 24 kΩ and 30 kΩ. The results are shown in the supplementary material (Fig. S10). Although, the mean R_{HRS} of the considered cycles, thereby, shifts to 26.92 ± 1.77 kΩ (above the mean R_{HRS} value of the TaO_x device), the SET and transition times of the ZrO_x device are only slightly reduced and still faster than the ones of the TaO_x device. Therefore, possibility (b) does not apply and possibility (a) is a reasonable explanation.

In our recent publication, several plausible limits of the switching speed are discussed.[10] Intrinsically, the speed is limited by the migration of oxygen vacancies, which can be described by the law of Mott–Gurney[19] or the model of Genreith-Schriever *et al.*[46] As a result, the switching speed would be limited by the reciprocal value of the phonon frequency multiplied by the hopping distance. The phonon frequency for both TaO_x and ZrO_x is in the THz regime.[47,48] Accordingly, SET times of hundreds of femtoseconds are plausible. Technologically, however, the heating and the charging time of the devices are the limiting factors. For the both devices, the RC time amounts to about 50 ps. This effect may have slowed down the measured SET and transition times, as observed in Ref. 11. The heating time is difficult to estimate, as it depends on many quantities such as the thermal conductivity, specific heat, mass density, and geometry of the heated

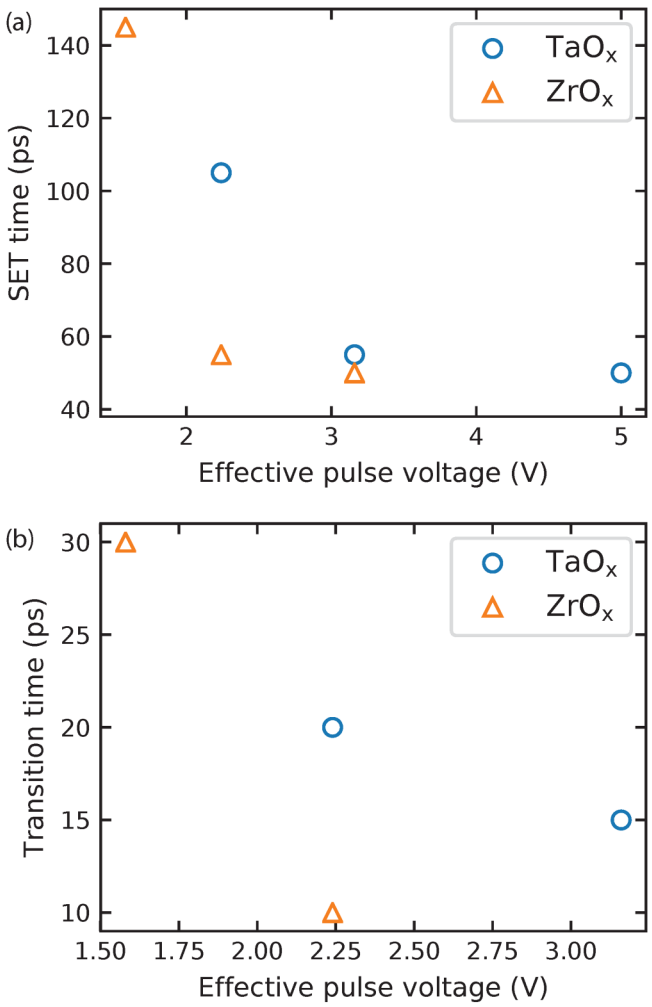

FIG. 5. SET time (a) and transition time (b) of the TaO_x (blue circles) and ZrO_x device (orange triangles) in dependence of the effective pulse voltage. Only the values for the SET time can be shown at 5.01 V for the TaOx device and at 3.16 V for the ZrOx device, because in these two cases both devices already switched within 50 ps. Therefore, the transition occurs in the time region below 50 ps, which cannot be recorded with our setup. Consequently, the transition time cannot be determined for these two cases.

region. All these factors have been considered in the finite element simulations of Ref. 10. The heating time for all combinations was below 120 ps. For the considered materials, a heating time of about tens of picoseconds is more likely. Therefore, the heating could also have decelerated the measured SET times. In this study, however, the switching speed is still limited by the setup, as the shortest observed SET time corresponds to the shortest pulse width. The charging and heating times may have delayed the measured SET and transition times; however, they do not prohibit SET times of 50 ps at a voltage of −5.01 V (TaO_x) or −3.16 V (ZrO_x). Both the switching time and the switching voltage are crucial requirements for memory technologies to become marketable. Current non-volatile memory technologies have significantly longer switching times and in the case of Flash also higher voltages are required.[2,49]

Identifying the intrinsic speed limit requires faster measurements. To this end, new approaches need to be investigated as electrical measurements tend to be limited by the capacitive charging time. This charging time can be reduced by employing smaller feature sizes.[10,33] The bandwidth of the coplanar waveguide structure would, however, suffer from smaller feature sizes. One experimental approach to overcome this issue are optical measurements, which provide signals in the THz regime. In lateral phase change memories, for example, switching times of about 1 ps have been observed by inducing an electrical field with a laser source.[50] Comparable studies for VCM devices are still missing and would require lateral structures as well.

Another aspect of ReRAM devices is their compatibility for neuromorphic applications.[12] In our previous study on HfO_x devices, it was shown that SET and RESET pulses with a high amplitude prohibit intermediate states, which would be required for neuromorphic applications.[45] It concludes that a ReRAM device requires transition times on the same order of magnitude as the used pulse width to become suitable for neuromorphic applications. The binary operations presented in this paper require high voltage amplitudes above 1 V. Similarly to the SET time, the transition time also depends exponentially on the applied voltage.[36] As a result, short transition times below 30 ps were measured due to the high effective pulse voltage. Therefore, there might be a trade-off between fast switching times (which require higher voltages) and the compatibility with neuromorphic applications (which require slow transition times). In another study on TiO_x devices, however, intermediate states became only achievable with shorter pulses.[13] Therefore, it might be possible to achieve multiple states with short pulses in the presented devices as well, which requires further investigation.

IV. CONCLUSION

By collecting and statistically evaluating a comprehensive data set, the transition from the HRS to the LRS of a TaO_x and a ZrO_x device could be measured on a picosecond timescale. This allows the precise determination of the voltage dependent SET kinetics between 50 ps and 250 ps. Both the measured switching speed of 50 ps and the transition from the HRS to LRS within 10 ps have not yet been reported for VCM-based devices. The SET kinetics of the ZrO_x device are faster than the ones of the TaO_x device, which is attributed to the lower migration barrier for oxygen vacancies in ZrO_x.

Additionally, two evaluation methods to determine the SET time at this timescales are compared. Determining the SET time by (i) evaluating the transmitted signal is more complex than (ii) determining the SET time by collecting a comprehensive data set and only evaluating the pulse width. Method (i) also becomes less reliable if the SET time approaches the charging time of the devices capacitance. At slower timescales, both methods yield similar results. The intrinsic switching speed limit of VCM-based devices, however, was not found. Further studies are therefore required to determine the absolute switching speed limit of VCM devices.

SUPPLEMENTARY MATERIAL

See the supplementary material for more information on the characterization of the devices (frequency domain measurements, endurance measurements) and the performance of the setup (exemplary pulses, pulse width preservation). It also includes more detailed statistics of the measurements.

ACKNOWLEDGMENTS

This work was in part funded by the German Research Foundation (DFG) under Grant No. SFB 917 and in part by the Federal Ministry of Education and Research (BMBF, Germany) in the project NEUROTEC (Project Nos. 16ES1134 and 16ES1133K). We thank Artem Zaidman and Stefan Leisten for their laboratory assistance.

REFERENCES

[1]R. Waser, R. Dittmann, G. Staikov, and K. Szot, Adv. Mater. **21**, 2632 (2009).
[2]J. J. Yang, D. B. Strukov, and D. R. Stewart, Nat. Nanotechnol. **8**, 13 (2013).
[3]M.-J. Lee, C. B. Lee, D. Lee, S. R. Lee, M. Chang, J. H. Hur, Y.-B. Kim, C.-J. Kim, D. H. Seo, S. Seo, U.-I. Chung, I.-K. Yoo, and K. Kim, Nat. Mater. **10**, 625 (2011).
[4]T. Ninomiya, Z. Wei, S. Muraoka, R. Yasuhara, K. Katayama, and T. Takagi, IEEE Trans. Electron Devices **60**, 1384 (2013).
[5]B. Govoreanu, G. Kar, Y. Chen, V. Paraschiv, S. Kubicek, A. Fantini, I. Radu, L. Goux, S. Clima, R. Degraeve, N. Jossart, O. Richard, T. Vandeweyer, K. Seo, P. Hendrickx, G. Pourtois, H. Bender, L. Altimime, D. Wouters, J. Kittl, and M. Jurczak, in *2011 IEEE International Electron Devices Meeting (IEDM)* (IEEE, 2011), p. 31.6.1.
[6]A. C. Torrezan, J. P. Strachan, G. Medeiros-Ribeiro, and R. S. Williams, Nanotechnology **22**, 485203 (2011).
[7]B. J. Choi, A. C. Torrezan, K. J. Norris, F. Miao, J. P. Strachan, M.-X. Zhang, D. A. A. Ohlberg, N. P. Kobayashi, J. J. Yang, and R. S. Williams, Nano Lett. **13**, 3213 (2013).
[8]B. J. Choi, A. C. Torrezan, S. Kumar, J. P. Strachan, P. G. Kotula, A. J. Lohn, M. J. Marinella, Z. Li, R. S. Williams, and J. J. Yang, Adv. Funct. Mater. **26**, 5290 (2016).
[9]C. Wang, H. Wu, B. Gao, W. Wu, L. Dai, X. Li, and H. Qian, Adv. Electron. Mater. **3**, 1700263 (2017).
[10]S. Menzel, M. von Witzleben, V. Havel, and U. Boettger, Faraday Discuss. **213**, 197 (2019).
[11]U. Böttger, M. V. Witzleben, V. Havel, K. Fleck, V. Rana, R. Waser, and S. Menzel, arXiv:2002.00700 (2019).
[12]M. A. Zidan, J. P. Strachan, and W. D. Lu, Nat. Electron. **1**, 22 (2018).
[13]S. Stathopoulos, A. Khiat, M. Trapatseli, S. Cortese, A. Serb, I. Valov, and T. Prodromakis, Sci. Rep. **7**, 17532 (2017).
[14]K. Skaja, C. Bäumer, O. Peters, S. Menzel, M. Moors, H. Du, M. Bornhöfft, C. Schmitz, C.-L. Jia, C. M. Schneider, J. Mayer, R. Waser, and R. Dittmann, Adv. Funct. Mater. **25**, 7154 (2015).
[15]C. Baeumer, C. Schmitz, A. H. H. Ramadan, H. Du, K. Skaja, V. Feyer, P. Muller, B. Arndt, C. Jia, J. Mayer, R. A. De Souza, C. M. Schneider, R. Waser, and R. Dittmann, Nat. Commun. **6**, 9610 (2015).
[16]A. Kindsmüller, C. Schmitz, C. Wiemann, K. Skaja, D. J. Wouters, R. Waser, C. M. Schneider, and R. Dittmann, APL Mater. **6**, 046106 (2018).
[17]Y. Ma, D. Li, A. A. Herzing, D. A. Cullen, B. T. Sneed, K. L. More, N. T. Nuhfer, J. A. Bain, and M. Skowronski, ACS Appl. Mater. Interfaces **10**, 23187–23197 (2018).
[18]S. Privitera, G. Bersuker, S. Lombardo, C. Bongiorno, and D. C. Gilmer, Solid State Electron. **111**, 161 (2015).
[19]S. Menzel, M. Waters, A. Marchewka, U. Böttger, R. Dittmann, and R. Waser, Adv. Funct. Mater. **21**, 4487 (2011).
[20]A. Marchewka, B. Roesgen, K. Skaja, H. Du, C. L. Jia, J. Mayer, V. Rana, R. Waser, and S. Menzel, Adv. Electron. Mater. **2**, 1500233 (2016).
[21]E. Yalon, S. Cohen, A. Gavrilov, and D. Ritter, Nanotechnology **23**, 465201 (2012).
[22]E. Yalon, I. Karpov, V. Karpov, I. Riess, D. Kalaev, and D. Ritter, Nanoscale **7**, 15434 (2015).
[23]J. Kwon, A. A. Sharma, C.-Y. Chen, A. Fantini, M. Jurczak, A. A. Herzing, J. A. Bain, Y. N. Picard, and M. Skowronski, ACS Appl. Mater. Interfaces **8**, 20176 (2016).
[24]S. Larentis, F. Nardi, S. Balatti, D. C. Gilmer, and D. Ielmini, IEEE Trans. Electron Devices **59**, 2468 (2012).
[25]S. Kim, S. Choi, J. Lee, and W. D. Lu, ACS Nano **8**, 10262 (2014).
[26]A. Siemon, S. Menzel, A. Marchewka, Y. Nishi, R. Waser, and E. Linn, in *2014 IEEE International Symposium on Circuits and Systems (ISCAS)* (IEEE, 2014), p. 1420.
[27]C. Hermes, M. Wimmer, S. Menzel, K. Fleck, G. Bruns, M. Salinga, U. Boettger, R. Bruchhaus, T. Schmitz-Kempen, M. Wuttig, and R. Waser, IEEE Electron Device Lett. **32**, 1116 (2011).
[28]P. Huang, Y. Wang, H. Li, B. Gao, B. Chen, F. Zhang, L. Zeng, G. Du, J. Kang, and X. Liu, IEEE Trans. Nanotechnol. **13**, 1127 (2014).
[29]M. Witzleben, K. Fleck, C. Funck, B. Baumkötter, M. Zuric, A. Idt, T. Breuer, R. Waser, U. Böttger, and S. Menzel, Adv. Electron. Mater. **3**, 1700294 (2017).
[30]W. Kim, S. Menzel, D. J. Wouters, Y. Guo, J. Robertson, B. Rösgen, R. Waser, and V. Rana, Nanoscale **8**, 17774 (2016).
[31]Y. Nishi, S. Menzel, K. Fleck, U. Boettger, and R. Waser, IEEE Electron Device Lett. **35**, 259 (2014).
[32]S. Menzel, U. Böttger, M. Wimmer, and M. Salinga, Adv. Funct. Mater. **25**, 6306 (2015).
[33]Y. Lu, J. H. Lee, and I.-W. Chen, ACS Nano **9**, 7649 (2015).
[34]Y. Guo and J. Robertson, Appl. Phys. Lett. **105**, 223516 (2014).
[35]P. Huang, B. Chen, Y. Wang, F. Zhang, L. Shen, R. Liu, L. Zeng, G. Du, X. Zhang, B. Gao, J. Kang, X. Liu, X. Wang, B. Weng, Y. Tang, G. Lo, and D. Kwong, in *2013 IEEE International Electron Devices Meeting (IEDM)* (IEEE, 2013), p. 22.5.1.
[36]K. Fleck, C. La Torre, N. Aslam, S. Hoffmann-Eifert, U. Böttger, and S. Menzel, Phys. Rev. Appl. **6**, 064015 (2016).
[37]C. La Torre, A. Kindsmueller, D. J. Wouters, C. E. Graves, G. A. Gibson, J. P. Strachan, R. S. Williams, R. Waser, and S. Menzel, Nanoscale **9**, 14414 (2017).
[38]A. Schoenhals, D. J. Wouters, A. Marchewka, T. Breuer, K. Skaja, V. Rana, S. Menzel, and R. Waser, in *2015 IEEE International Memory Workshop (IMW)* (IEEE, 2015), p. 73.
[39]J. W. McPherson, J. Kim, A. Shanware, H. Mogul, and J. Rodriguez, IEEE Trans. Electron Devices **50**, 1771 (2003).
[40]I. Kaerkkaenen, A. Shkabko, M. Heikkila, M. Vehkamaki, J. Niinisto, N. Aslam, P. Meuffels, M. Ritala, M. Leskela, R. Waser, and S. Hoffmann-Eifert, Phys. Status Solidi A **212**, 751 (2015).
[41]R. Devanathan, W. Weber, S. Singhal, and J. Gale, Solid State Ionics **177**, 1251 (2006).
[42]S. Choi, J. Lee, S. Kim, and W. D. Lu, Appl. Phys. Lett. **105**, 113510 (2014).
[43]R. Nakamura, T. Toda, S. Tsukui, M. Tane, M. Ishimaru, T. Suzuki, and H. Nakajima, J. Appl. Phys. **116**, 033504 (2014).
[44]W. Kim, S. Menzel, D. J. Wouters, R. Waser, and V. Rana, IEEE Electron Device Lett. **37**, 564 (2016).
[45]F. Cüppers, S. Menzel, C. Bengel, A. Hardtdegen, M. von Witzleben, U. Böttger, R. Waser, and S. Hoffmann-Eifert, APL Mater. **7**, 91105 (2019).
[46]A. R. Genreith-Schriever and R. A. De Souza, Phys. Rev. B **94**, 224304 (2016).
[47]X. Zhao and D. Vanderbilt, Phys. Rev. B **65**, 75105 (2002).
[48]H. Ono and K. Koyanagi, Appl. Phys. Lett. **77**, 1431 (2000).
[49]S. Yu and P.-Y. Chen, IEEE Solid State Circuits Mag. **8**, 43 (2016).
[50]P. Zalden, M. J. Shu, F. Chen, X. Wu, Y. Zhu, H. Wen, S. Johnston, Z.-X. Shen, P. Landreman, M. Brongersma, S. W. Fong, H.-S. P. Wong, M.-J. Sher, P. Jost, M. Kaes, M. Salinga, A. von Hoegen, M. Wuttig, and A. M. Lindenberg, Phys. Rev. Lett. **117**, 067601 (2016).